Progress Report 2014 and Beam Request for 2015

Muon Capture on the Deuteron

The MuSun Experiment

PSI Experiment R-08-01, spokespersons P. Kammel, C. Petitjean, A.A. Vasilyev

MuSun Collaboration [1]

Petersburg Nuclear Physics Institute – University of Washington (Seattle) – Paul Scherrer Institut – University of Kentucky – Boston University – Regis University – University of South Carolina

http://muon.npl.washington.edu/exp/MuSun

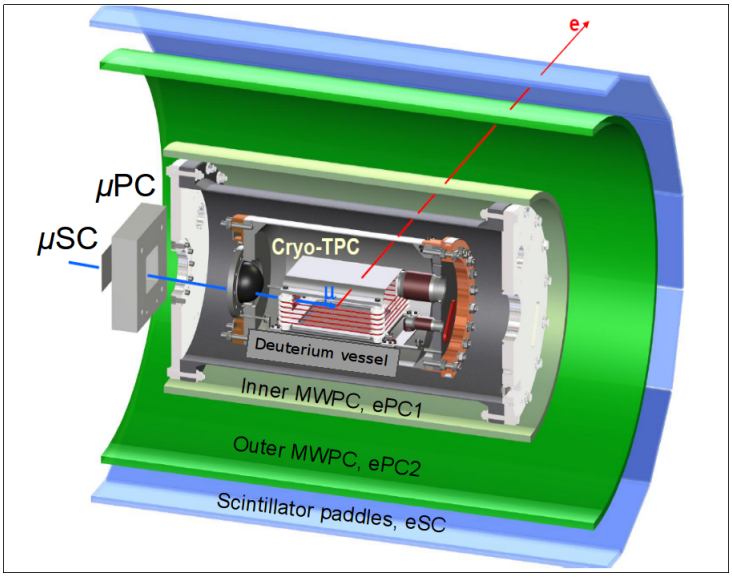

Figure 1: MuSun detector model. Muons pass through entrance detectors to stop in a deuterium target TPC. The decay electron is detected in two cylindrical wire chambers (green) and a 16-fold segmented scintillator array.

Contents

1 Overview **3**
- 1.1 Introduction . . . 3
- 1.2 Progress 2014 . . . 3
- 1.3 Remaining MuSun Program . . . 3

2 Physics Run R2014 **4**
- 2.1 Chronology . . . 4
- 2.2 Beam Tuning . . . 5
- 2.3 System Performance and First Results . . . 7
  - 2.3.1 TPC . . . 7
  - 2.3.2 CHUPS and Chromatography . . . 8
  - 2.3.3 Other System Improvements . . . 9

3 Data Analysis **10**
- 3.1 Software Framework . . . 10
  - 3.1.1 Data Processing . . . 10
  - 3.1.2 Monte-Carlo Simulations . . . 11
- 3.2 Statistics . . . 12
- 3.3 Systematics . . . 13
  - 3.3.1 Purity . . . 13
  - 3.3.2 Interferences . . . 15

4 Beam Time Request 2015 **17**

1 Overview

1.1 Introduction

The final result of the MuCap experiment [2] was recently published, followed, in 2014, by a technical paper describing the key enabling instrument for achieving this goal, an ultra-pure hydrogen time projection chamber (TPC) [3]. A draft concerning our precision measurement of the formation rate of muonic hydrogen molecules, an important ingredient to the MuCap analysis, is under collaboration review and will be submitted this month. MuCap measured the rate of muon capture on the proton to determine g_P, the weak-pseudoscalar coupling of the proton. This first precise and unambiguous measurement of g_P confirms a fundamental prediction of low energy QCD.

The good agreement between the MuCap result and theory demonstrates that all parameters entering the *one-nucleon* weak amplitudes are well under control. This allows the MuSun experiment to extend this program with a precise determination of the strength of the weak interaction in the *two-nucleon* system, using the process

$$\mu + d \to n + n + \nu. \tag{1}$$

MuSun will determine the sole unknown low-energy constant involved in modern – QCD-based – effective field theory (EFT) calculations of weak nuclear reactions. The anticipated precision is 5 times better than presently available from the two-nucleon system and will be essential for calibrating these reactions in a model-independent way. This will provide a benchmark for extending the EFT method to more complicated few-body processes. Regarding the family of two-nucleon weak-interaction processes, muon capture will provide unique constraints on electro-weak astrophysical processes of fundamental importance, like pp fusion or νd scattering, whose rates have never been measured directly.

MuSun measures Λ_d, the capture rate from the doublet hyperfine state of the muonic deuterium atom in its 1S ground state, by determining the negative muon decay rate λ_- in a time projection chamber filled with ultra-pure deuterium gas at cryogenic temperatures. The capture rate is derived from the difference

$$\Lambda_d \approx \lambda_- - \lambda_+ \,, \tag{2}$$

where λ_+ is the positive muon decay rate [4]. As sketched in Fig. 1, the detector consists of muon detectors (muSC, muSCA, TPC), electron detectors (ePC1/2, eSC) and neutron detectors (not shown). For a more detailed discussion of the novel experimental strategy, we refer to our earlier Reports. The physics aspects of this field are covered in review [5].

1.2 Progress 2014

The year 2014 was an excellent one for MuSun. The new TPC was constructed according to a tight schedule to allow thorough testing and preparation before the run. It performed flawlessly during the whole production period. The continuous purification system (CHUPS) maintained excellent purity at the 1 ppb level, which could be monitored by a significantly-improved gas chromatography system that led to a consistent result. The TPC cryogenic preamplifiers [6] also worked without problems and now have sufficient resolution to provide in-situ monitoring of the critical gas purity. The PSI accelerator delivered stable beam, but the secondary muon beam still needed improvements to match the πE3 quality we had a few years ago. We were forced to dedicate some time and effort to scanning the beam, but by the middle of the run this problem was resolved with a new collimator design.

The analysis also made significant progress, and we address the most challenging aspects in a dedicated section of this report.

1.3 Remaining MuSun Program

MuSun plans to measure Λ_d with a precision of better than 1.5%, which amounts to $\delta\Lambda_d = 6$ Hz. The capture rate is derived according to equation (2). The positive muon lifetime is well-known from MuLan

with 1 ppm precision. Thus the uncertainty in $\delta\Lambda_d$ is dominated by the MuSun measurement of λ_- in deuterium. If we assume equal statistical and systematic contributions to the final result, the statistics requirement for the number of fully reconstructed $\mu - e$ decays N becomes

$$N > 2(\lambda_-/\delta\lambda_-)^2 \tag{3}$$

For $\delta\lambda_- = \delta\Lambda_d$, these are 1.2×10^{10} events. Assuming an optimal run in 2015, we collected 6×10^9 events in run 2014 and expect 8×10^9 events from run 2015, in total 1.4×10^{10} events. Due to the fusion interference discussed below, the lifetime fits will start after 1 μs, which reduces the statistics by 37% to $N_{fit} = 0.9 \times 10^{10}$. Thus, if the 2015 run matches the 2014 data taking efficiency, we can come close enough to the desired statistics. Of course, this estimate does not include any contingency, as any increase of the systematic uncertainty beyond 3 Hz would deteriorate the estimated final error. In the statistics estimate, we have only included the golden runs 2014 and hopefully 2015. Run 2013 will serve as an important check of impurity corrections, as it had a higher impurity level due to a failure in our purification system. The initial commissioning run in 2011 was performed before the gas purification and diagnostics were in their final optimized state, so it will have larger systematic uncertainties (c.f. Fig. 9).

In conclusion, the collaboration is optimistic that the final statistics goals of MuSun can be achieved with a 12-week run in 2015. However, we request the option for a shorter running period dedicated to systematic studies in 2016.

2 Physics Run R2014

2.1 Chronology

During the 2014 production run, over six full weeks of μ^- data and one week of μ^+ data were accumulated. An additional week was dedicated to systematic studies.

The success of the run was due, in part, to ample preparation. In May 2014, several weeks at PSI were dedicated to constructing, installing, and testing a new and upgraded TPC (Sec. 2.3.1). By ensuring the TPC could be operated at nominal conditions, hold appropriate voltages, and obtain an adequate resolution in advance, we were able to quickly begin production data taking in the summer.

On July 31, the clock frequencies were blinded from the collaboration and μ^- production was started. Stable temperature and pressure conditions of 31 K and 5.1 bar were reached and maintained for the deuterium gas. In the first few weeks, the grid HV occasionally dropped by a few hundred volts due to sparking, but eventually a stable grid voltage of 3.5 kV and a cathode voltage of 80 kV were reached.

Once the stabilization of detectors was achieved in standard conditions, extra time could be dedicated to optimization of the data rate. Several attempts to increase the data rate with DAQ improvements included mounting a new solid-state drive on the main DAQ computer and changing the output file size. In the first week of production data, updating the Linux kernel to overcome a motherboard issue was able to increase the DAQ performance, and reduce the deadtime to 10%.

Optimization of the beam tune continued for several weeks into production (see section 2.2). After scanning the beam upstream and designing a new collimator, this problem was largely solved by Sept. 3.

On August 18, the first scheduled shutdown began. During this time the clock stability was measured, and additional memory was added to the DAQ computer.

A clocked entrance trigger was installed on a 2.5 kHz clock to replicate a muon in the entrance detectors for background studies. In addition to running the clock throughout the second half of production, an eight-hour shift with an increased rate of 20 kHz was taken to accumulate significant statistics during a shorter period.

On September 17, a magnet was installed to provide a spin-rotation field for positive muons, and we switched to data-taking with μ^+. A week of data was accumulated with smooth running conditions. After 10^9 events were acquired, the beam polarity was switched back to μ^- for one more week, followed by a week of systematic studies.

To increase sensitivity for in-situ impurity detection in the TPC, data was taken for three days at 50% of nominal density. This reduction in density provides a clear separation between the recoil energies from muon capture on impurities and the ^{3}He recoil energies. An additional three days of data were collected at the reduced density with a temperature of 28 K. A decrease in temperature should lead to a reduction in impurity captures and acts as a test for the in-situ measurement of gas impurities (Sec. 3.3.1).

In summary, the successful 2014 run resulted in over 6×10^9 good μ^- and 1×10^9 μ^+ stops after applying pileup protection, a fiducial volume cut, and an electron track requirement. These cuts are roughly equivalent the final cuts, and the remaining stops are representative of the final statistics. The accumulation of the statistics throughout the run can be seen in Fig. 2.

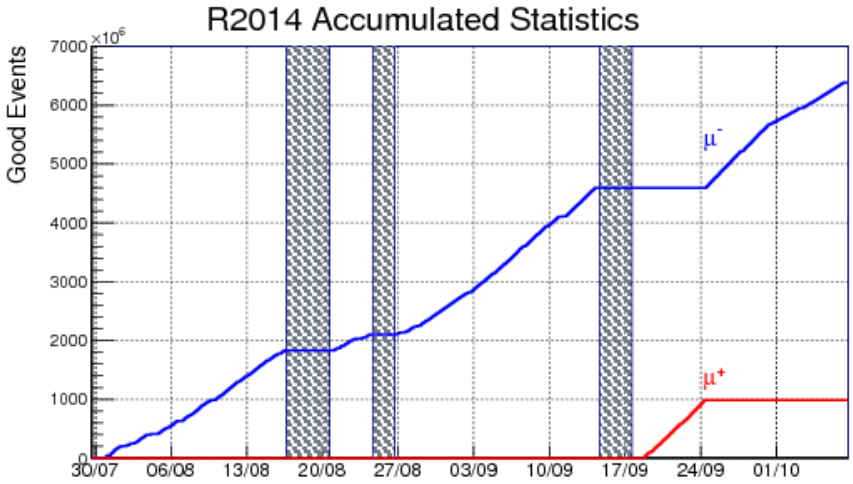

Figure 2: Number of fully reconstructed decay events acquired over the run period, after all selection cuts were applied, for R2014. The gray bands indicate two beam-less periods due to scheduled shutdowns and one period for target exchange. The available beam could be utilized with high efficiency, averaging a collection rate of 10^9 good events per week.

2.2 Beam Tuning

As mentioned above, the MuSun detector and gas system were ready for production data taking after a record short set-up time. Given the complexity of the apparatus, this was only possible because the experiment had been permanently installed in the dedicated πE1.2 area on rails, so that it could be retracted to make space for other, smaller experiments without major disturbance.

However, for efficient production it was critical to establish beam conditions of similar quality as we had in πE3, which was not trivial. Below we document our efforts, in the hope that this will also assist other πE1 users interested in high-quality low-energy muon beams.

The user-accessible beam line outside the shielding wall consists of the following main elements (Fig. 3). Muons are kicked and electrons are separated in the vertical plane by the $\pm$12 kV MuLan RF-kicker and the 190 kV $E \times B$ separator, respectively, before being bent towards πE1.2 with ASK 51. The RF-kicker establishes a muon-on-request beam to reduce pile-up and background, by deflecting the beam after a muon trigger. The extinction factor characterizes by how much the beam can be suppressed in this mode. A critical point in the optics is the double focus in the center of this bending magnet (ASK SLIT), which allows vertical collimation to stop electrons and kicked-off muons and provides horizontal achromaticity at the final target location downstream. The separation can also be done at the next focus (SLIT3), but the image is expected to be sharper right after the separator.

In 2013 we ran with a PSI-designed, manually operated collimator at ASK SLIT, but the beam

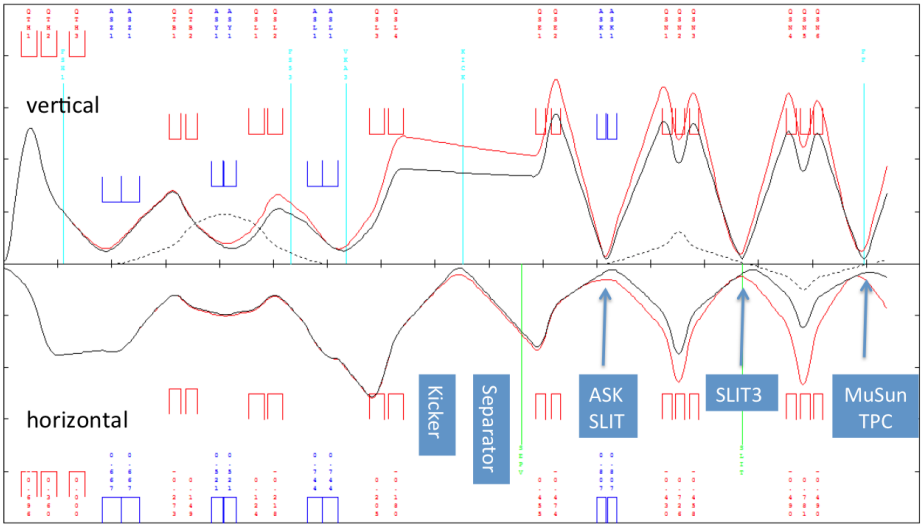

Figure 3: Typical beam envelopes as calculated by TRANSPORT.

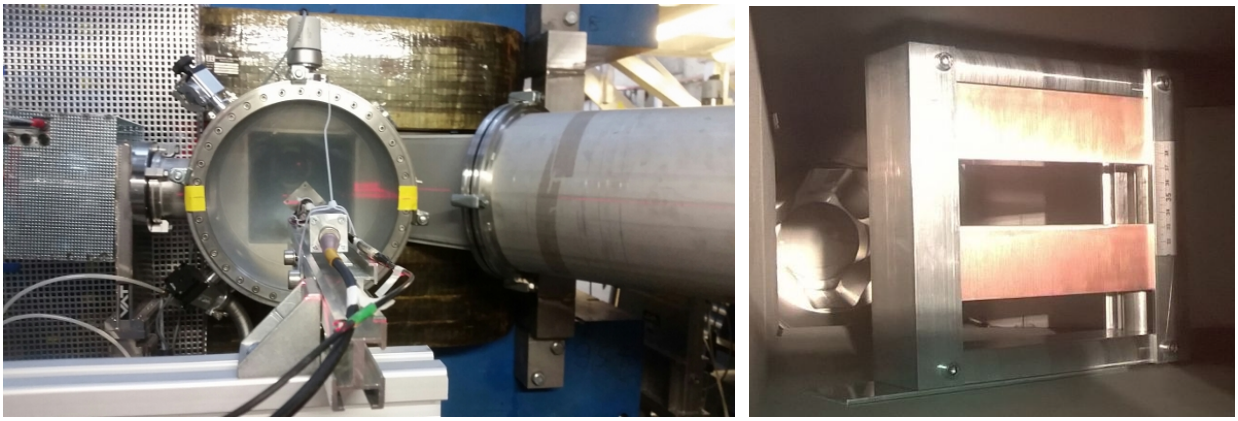

Figure 4: Left: Setup for beam scanning behind ASK51. Right: New collimator inside ASK51 vacuum.

extinction and beam electron contamination were poor (c.f. Fig. 9). In 2014, after an initial unsuccessful attempt with the old collimator, we started without a collimator in ASK SLIT, but suffered similar problems. Attempts to carefully tune the beam line elements and to optimize the beam by lowering the apparatus to symmetrize the stopping distribution did not lead to much progress.

Thus we decided to perform a dedicated beam study with an upgraded scanning system, provided by K. Deiters, right after the ASK51 magnet, by replacing its back flange with a thin window (Fig. 4). These studies provided firm information on the muon and electron beam positions and profiles as functions of separator and kicker voltage at the critical ASK SLIT position. After the collimator was installed again and did not produce the expected results, we realized that its left support partially interfered with the beam. A new collimator (Fig. 4) was designed during the run, which provided 3 times better electron suppression and muon extinction (Fig. 5). Further improvement on electron suppression likely involves larger $E \times B$ deflection, as provided by the horizontal MSR spin rotator. However, space limitations would require a significant beam line redesign to benefit from such a solution. The performance is summarized in Fig. 5 and Table 1.

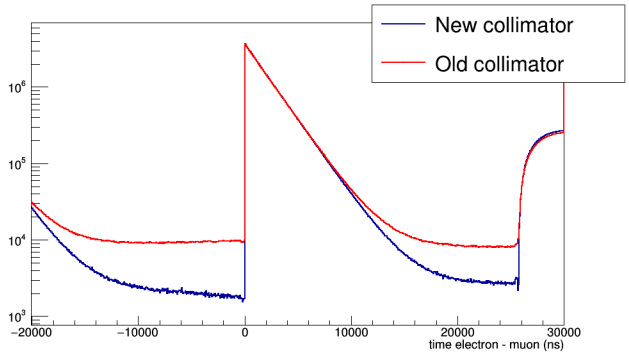

Figure 5: Lifetime histogram before and after fixing the collimator in the bending magnet. The background, which was dominated by beam electrons, gets reduced by a factor of 3.

data set	R_μ	R_μ^{kicked}	$R_{stop\ in\ TPC}$	$R_{\mu-e\ event}$	R_{acc}	Extinction
μ^- no coll.	64	25.5	5.1	1.9	1.1	53
old coll.	64	26.5	4.6	1.7	0.96	67
new coll.	53	26	5.7	2.4	0.37	160
μ^+	46	24	5.5	2.5	0.3	50

Table 1: Characteristic rates in kHz and extinction factor for different collimator configurations. The beam momentum was 39 MeV/c, with a momentum bin 3% for μ^-, 2% for μ^+. R_μ is the incident muon rate, R_μ^{kicked} the rate after the RF-kicker and R_{acc} the accidental rate in the $\mu - e$ spectrum, Fig. 5.

2.3 System Performance and First Results

2.3.1 TPC

Several major upgrades were implemented in the R2014 cryo-TPC, including a new Frisch grid, improved high-voltage structure, and high-precision temperature sensors. It operated at stable conditions throughout the run, with 80 kV on the cathode and 3.5 kV on the Frisch grid.

In R2013, a new grid construction was used, consisting of gold-plated tungsten wires tensioned and soldered to a solid tungsten frame. The frame showed characteristic improvement in voltage stability and signal amplitude, but suffered a mechanical failure during a temperature cycle near the end of the run. The tensioned wires and silver coating began peeling from the frame due to stresses from mismatched temperature coefficients. For R2014, a new grid was manufactured at the University of Washington (UW). The new composite grid frame, designed in collaboration with the PSI detector group, has tungsten cross bars along the direction of the gold-plated tungsten field wires, while the rest of the mechanical structure and soldering pads are constructed from stainless steel. This construction allowed us to keep the wires tensioned at cryogenic temperatures, while soldering them on stainless steel and thus eliminating the need for a silver plating.

Four composite frames were precision machined at UW with wire electrical discharge machining (EDM). The tungsten bars were high-temperature soldered to the stainless steel by the PSI workshop. Three complete frames with tensioned wires were produced by the PSI detector group, so a spare was readily available during the run. In addition, the fourth frame was used in temperature cycling tests, which demonstrated reliability before production beam time had started.

The new Frisch grid design implied a redesign of several other TPC components. The Macor high-voltage posts were changed to a simpler cylindrical design for ease of machining. A new set of silver-plated 1.524 mm diameter tungsten wires was produced for the field cage, with 0.5 mm silver wires at the entrance. PNPI built a new cathode consisting of a silver foil held between two stainless-steel frames.

New PT-100 temperature sensors were calibrated at PNPI and installed in the center and on both

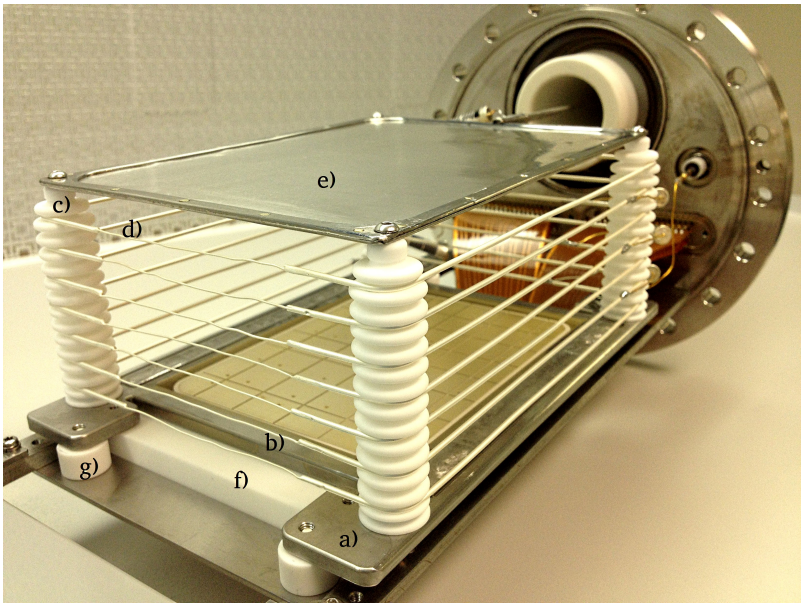

Figure 6: Assembled TPC for the R2014 in the clean room of the PSI detector group. a) New composite grid with b) tungsten cross bars. A new high-voltage structure with c) simplified Macor posts, d) silver-plated tungsten field wires, and a e) silver cathode. The new grid design also implied a new support structure for the f) anode and the g) grid.

flanges of the TPC vessel. The calibration enabled reliable temperature readout with at least 0.1 K accuracy. In addition, a neon condensation temperature sensor was installed to cross-check the PT-100's.

In May, with help from the PSI detector group, the TPC was fully constructed and commissioned at PSI. Most of the assembly was done in the clean room of the PSI detector group. After closing the pressure vessel and testing all electrical connections, the detector was installed in πE1 and tested at its nominal temperature and pressure. All components survived temperature cycling, we found no leaks of the vacuum seals, and the grid high voltage was found to be stable up to 3.5 kV, which is close to full transparency. A photograph of the new TPC can be seen in Fig. 6.

During the run, we were able to keep stable voltages at nominal conditions, and we had no mechanical failures after several temperature cycles. As an additional protection against sparking, the input resistors on all preamplifiers were changed to metal electrode face-bonded (MELF) type resistors. All 48 preamplifier [6] channels performed with 10 keV resolution, equivalent to 250 electrons RMS, for the duration of the run.

2.3.2 CHUPS and Chromatography

The required gas purity level of 1 ppb is achieved and maintained by our Cryogenic Hydrogen Ultra-high Purification System (CHUPS) [7]. CHUPS provides the TPC with a continuous flow of deuterium of up to 5 liters per minute, purified by Zeolite filters. For this year's run, these filters were equipped with temperature-controlled heaters, allowing for online regeneration. Saturated Zeolite absorbers were the cause of last year's increased gas-impurity level [8].

The purity level of the deuterium gas is measured by a gas chromatography system, which complements the analysis of nuclear capture recoils in the TPC (Sec. 2.3.1). A conventional gas chromatograph has a sensitivity of a few ppm. Our system boosts the sensitivity by cryogenic accumulation of impurities in an absorption bed. In addition, great care is taken in sampling the gas. Since last year, the system was directly connected to the TPC and CHUPS, avoiding the uncertainties introduced by sample volumes. The 2014 upgrades included the installation of a stabilized current supply for the heat conductivity detector

and a custom amplifier with variable gain and full digital readout [9]. Several measurements during the the 2014 run showed a stable level of nitrogen impurities around 1 ppb (Tab. 2).

Date	27-07	28-07	29-07	31-07	31-07	18-08	02-10	04-10	06-10
N_2 level (ppb)	1.60	1.00	1.20	1.30	1.20	0.7	0.60	0.60	0.50

Table 2: Nitrogen impurities during the 2014 run as measured by the gas chromatograph. Nitrogen impurities are our main concern, as the vapor pressure of N_2 at 31 K still yields concentrations > 10 ppb.

An important milestone was a careful calibration of the gas chromatography system. Previous attempts based on the saturation pressure of nitrogen around 30 K or using static sample volumes failed to provide consistent results. Therefore, a sample volume with ppm levels of nitrogen was connected to the CHUPS system with a precision mass flow controller, allowing us to dynamically set the gas purity to a desired level. Fig. 7 shows the expected versus measured impurity levels of the calibration measurements. The gas analyzer shows excellent linearity down to the ppb level. There is a 1 ppb offset which can be attributed to the purity of the *clean* gas. A residual 1 ppb can be due to a small level of impurities introduced by the gas mixing system or sample lines. Therefore, our gas chromatograph gives us an upper limit on the impurity level in the system. For the 2014 run, the limit on nitrogen impurities from this system is 0.97(51) ppb (nitrogen).

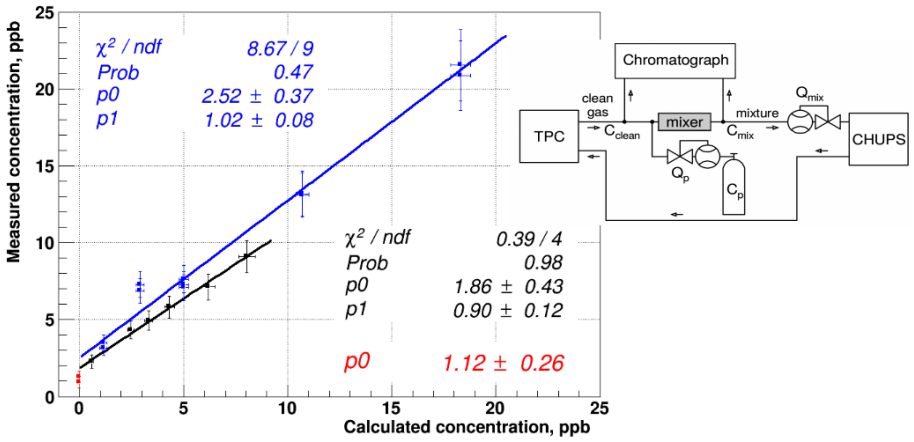

Figure 7: With the gas mixer, the nitrogen concentration in the system is increased at the ppb level and subsequently analyzed by the gas chromatograph. The expected versus measured concentrations were fitted with $C_{measured} = p1 * C_{calculated} + p0$. The gas nitrogen concentration with the mixer bypassed is measured to be 1 ppb (red).

2.3.3 Other System Improvements

No major changes were made to the data acquisition system for this run. However, there were a number of incremental improvements, such as the installation of a linear power supply on one electronics crate to reduce the switching noise interference that has been seen on the ePC signals; we also optimized the livetime of the system, regaining the $\sim 90\%$ level that was typical in MuCap.

In last year's report [8], we described work that was done to inspect the electron scintillator hodoscope for optical defects and to estimate the number of photoelectrons per minimum-ionizing pulse. We did not find any evidence for optical defects, and the number of photoelectrons was estimated to be ~ 50, so we

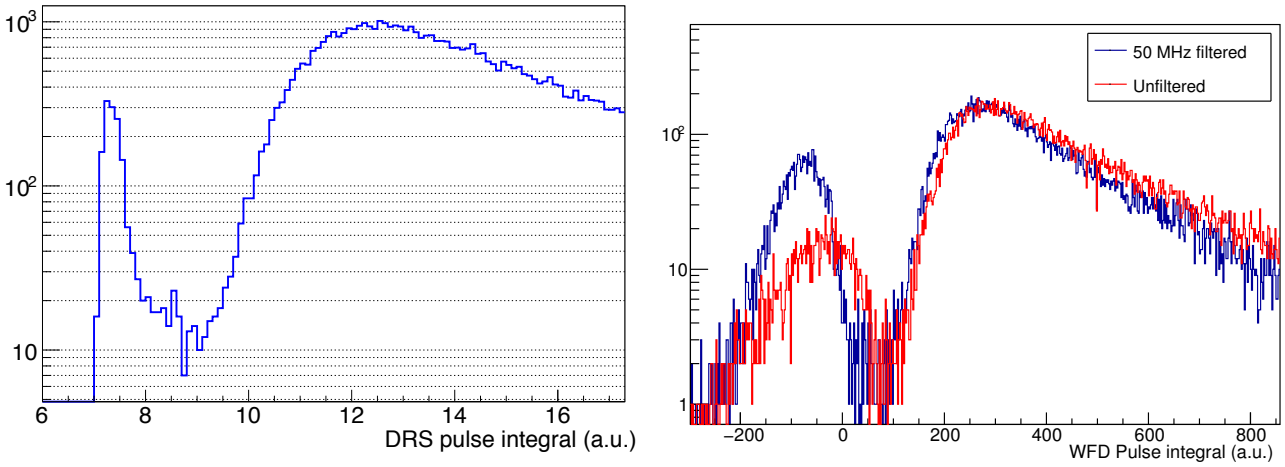

Figure 8: Electron detector pulse height resolution recorded for through-going cosmic ray muons, showing a separation between the noise and the minimum-ionizing signal. On the left is the result with a PSI DRS4 device; the plot on the right uses the standard MuSun electronics, both with and without an integrating filter that limited the analog bandwidth to 50 MHz.

concluded that any problems in the observed signal-to-noise ratio from the detector must be electronic rather than optical.

We continued this investigation before the 2014 run. We set up an experiment where one of the liquid scintillator neutron detectors was used as a trigger, and the response of the eSC to through-going cosmic ray muons was measured in coincidence with it. In this way, we measured the separation between minimum-ionizing events and the noise peak. We recorded these signals first with a PSI DRS4 evaluation board and then with the standard MuSun digitizers, and the separation was substantial in both cases, as shown in Figure 8. In fact, the separation was almost the same for the two devices, implying that the digitizer was not a limitation. This separation was obtained using simple analysis tools, not the full MuSun framework. Initially, the separation obtained with the full analysis software was substantially worse; after adjusting some software timing offsets and coincidence requirements, it improved dramatically. Consequently, we were able to show that the electron scintillator detector and its electronics are capable of good resolution.

We have improved our quality assurance by enhancing the computational power of the cluster used for near-real-time analysis. The online computer copied every data file to a disk accessible from this cluster. Monitoring scripts sampled those files, running a complete offline analysis on all events in selected files. When an analysis task finished with a file, it selected the most recently copied good run to analyze next. We were able to analyze 25% of the data with a lag time of five hours. Besides checking for data integrity, this was useful in monitoring impurity captures and electron backgrounds. The disk used by the near-real-time cluster was used as a source to copy all the acquired data to mass storage at the Texas Advanced Computing Center (TACC) as well as to the PSI archive. These copies were able to keep up with the data-taking rate.

3 Data Analysis

3.1 Software Framework

3.1.1 Data Processing

The analysis framework for MuSun data is written in C++, using ROOT and the modular MIDAS software developed at PSI. Analysis proceeds in multiple stages, with each stage processing increasingly

higher-level physical objects. In the first stage, raw information from detectors is translated into objects with physical significance, such as electron or muon tracks. In the second stage, these physical objects are correlated in order to produce the decay time distributions that are fitted to extract the muon lifetime. High-level systematic checks are also performed in the second stage. The MuSun analysis is performed with the absolute clock frequency blinded, and additional blinding between positive and negative muon data is implemented in software. For high-statistics analysis, MuSun has applied for and been granted an allocation (TG-PHY060011N) on the Stampede cluster at the Texas Advanced Computing Center for 160,000 service units (CPU-hours) during the 2015 calendar year.

Significant upgrades to the analysis chain include the electron and muon tracking, and treatment of the muon entrance detectors. The electron tracking framework is now flexible and comprehensive, allowing for any combination of detectors and cuts to be systematically studied. Alternative algorithms for muon tracking (see Sect. 3.3.2) have been developed with the purpose of minimizing interference from muon-catalyzed fusion. In R2014, DAQ changes were made to record occasional "fake" muon entrance triggers while all other detectors are read out as normal, with the purpose of studying backgrounds unrelated to beam muons. The code that processes the entrance detectors was upgraded to handle and separate these events, as well as to provide better diagnostics and systematic studies for normal events.

The importance of the new, more flexible electron track definition was crucial in understanding–and fixing–a large oscillation in the early-time residuals of our lifetime fits, which was evident in the R2011 data set [8]. Originally we defined the electron time as the average of the TDC times derived from discriminators of a 4-fold coincidence in the scintillator barrel (eSC). In R2011, the early-time residuals obtained with this definition were characterized by large (10 sigma), irregular oscillations. Using the new modular analysis approach, we examined lifetime residuals produced by *single* tubes. Viewed in this way, the damped oscillations are very regular and are particularly large (30 sigma) for the signals coming from one of the four LeCroy Discriminator modules. Fortunately, the eSC PMT signals are also read out with 500 MHz waveform digitizers (WFDs) running on an analog trigger. To solve the problem, we changed the electron definition to use the raw, analog WFD triggers, without making any cuts on the digitized waveform, which minimized the early time oscillations after 250 ns. At later times, the TDC and WFD views of the data are identical. Several questions remain concerning the origin of this noise. It came too early to be associated with the kicker transition itself, but may have been associated with the formation of the kicker trigger. A full understanding of what happened is probably impossible because we have moved to πE1, where the problem did not show up again.

3.1.2 Monte-Carlo Simulations

The MuSun Monte Carlo simulation chain is well-developed and has become a powerful tool to aid development of the muon track reconstruction in the TPC as well as to produce results for certain systematic effects where data-driven only checks are difficult. We have generated large data samples of 2×10^9 events each of μ^+ and μ^- entrances using the Lonestar cluster at TACC. On this cluster, a single job of 2×10^6 events took 80 minutes for GEANT, 85 minutes for the detector response, two hours 20 minutes for the low level first pass reconstruction, and 45 minutes for the high level second pass, for a total time of just under six hours. Since we run 1000 jobs in parallel, this is the total time it takes to produce each of these large datasets. Lonestar has been retired, and part of our grant on Stampede, which is twice as fast as Lonestar, includes time for substantially larger Monte Carlo datasets. In addition to increasing statistics, we need to create samples reflecting the different detector configurations. The lower noise of the new electronics used since 2013 substantially improves the TPC energy resolution and permits the use of a lower trigger threshold. The most recent large statistics sample simulated the conditions of 2011.

While large Monte Carlo samples are needed in order to check for general systematic problems in the analysis, there are specific issues that can be checked with targeted Monte Carlo data samples. In particular, this simulation work has been focused on the following three aspects: fusion interference, electron interference, and capture recoil background.

- **Fusion Interference**
  To select the muon stops in deuterium gas, we apply fiducial volume cuts, vetoing events that stop in the outermost row of pads and vertical borders of the TPC. However, muon-catalyzed fusion products can push a muon stop from outside to inside of the fiducial volume or vice versa. When there is a fusion, the muon must have survived long enough to cause the fusion, and thus, if there is a net migration, the measured muon disappearance rate will be affected. To check the scale of this event migration, we generated 2×10^7 μ^- events and processed them through the detector response with and without fusion products. Analyzing the simulated data and applying the fiducial volume cuts, the difference of lifetime fits between the two datasets gives the scale of fusion interference. Using our previous tracking algorithm we found a significant change in the μ^- disappearance rate compared to our systematic error budget. Because of this we have developed a new tracker (described in Sec. 3.3.2) to reduce this systematic correction.

- **Electron Interference**
  The Michel electron deposits energy in the TPC, which may modify the observed parent muon track. This is called electron muon track interference. Like fusion interference, this extra energy from the electron depends on the decay electron direction and time and, in a time dependent manner, can change the tracking algorithm's decision as to whether or not the parent muon was an accepted muon stop. This results in a direct error in the lifetime measurement. To study this effect we simulated 2×10^7 μ^+ events in GEANT4 and processed this dataset in the detector response with and without Michel electron energy deposition in the TPC. Differences in selecting muon stops should be caused strictly by electron interference. We found a small but non-negligible change in the observed disappearance rate, which we are currently comparing with a data-driven approach.

- **Neutron scattering**
  Neutrons are produced in $\mathrm{d}\mu^-\mathrm{d} \rightarrow \mu^- + \mathrm{n} + {}^3\mathrm{He}$ fusion events as well as through muon capture on deuterium, $\mu^- + d \rightarrow n + n + \nu_\mu$. The neutron energy distribution from muon capture is far from three-body phase space; we generate the neutron energy distribution according to a theoretically calculated spectrum. Neutrons have a relatively large scattering cross section on deuterium, and the recoiling deuteron will deposit its energy in the TPC. The deuteron recoil spectrum extends up to several MeV and could contribute to the impurity signal described in Sec. 3.3.1. As a quick check to see how large this contribution is, we generated Monte Carlo events consisting of single neutrons placed randomly in a"stop" pad and looked for recoil deuterons depositing energy in the TPC. We find a contribution to the impurity signal region of the delayed energy spectrum comparable to the capture yield for ppb-level impurities. Thus, this is a contribution which must be better quantified. The recoil energy and spatial distributions can be predicted by the Monte Carlo calculations and will be used in the comparison with data.

3.2 Statistics

MuSun has accumulated production data sets R2011, R2013, and R2014, in three beam periods since 2011. The data set R2011 was the first production data run in the πE3 area, demonstrating a fully functional experiment. However, our highly sensitive purity diagnostics could only be implemented after this run. Following several significant TPC upgrades motivated by improvements to impurity monitoring and migration of the experiment to the πE1 area, the collection of R2013 was hampered by accelerator downtime as well as delays due to detector malfunction. Importantly, though, a measurement with nitrogen-doped gas at 1950 ppb and 525 ppb was performed to calibrate the impurity detection methods. The summer beam period resulting in data set R2014 was very successful. The full data set from all three runs has been analyzed with a single muon tracking algorithm and simplified electron track identification. More complex algorithms and thorough examination have been performed on the R2011 data set. The analysis framework has been upgraded to reflect recent hardware changes and is now ready for a full-

statistics pass through the R2013 and R2014 data sets. See Table 3 for the accumulated statistics by beam period.

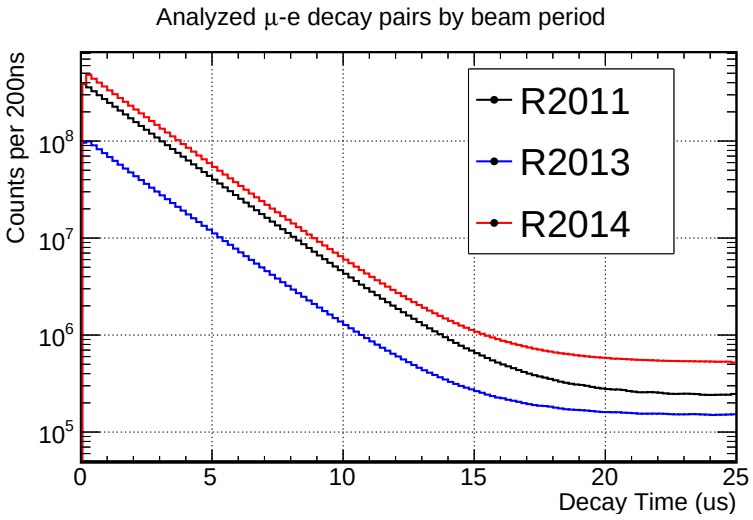

Data set	μ^-	μ^+
R2011	4.5×10^9	0.5×10^9
R2013	1.2×10^9	0.2×10^9
R2014	6.0×10^9	1.0×10^9

Table 3: Accumulated muon decays after all detector cuts. A conservative fit start time of 1000 ns would effectively reduce these totals by 40%.

Figure 9: Time distribution of analyzed $\mu^- - e$ decay pairs for each of the production MuSun datasets.

3.3 Systematics

We limit the discussion to two topics that are considered to be most critical for the experiment.

3.3.1 Purity

The gas impurities of concern in our cryo-TPC are oxygen and nitrogen. With the capture rate of negative muons much larger than on deuterium, the shift in the measured Λ_d is approximately 2 Hz/ppb for nitrogen and 1 Hz/ppb for oxygen. In addition, the expected nitrogen concentration at the vapor pressure at 31 K is still $>$ 10 ppb. Therefore, CHUPS continuously purifies the deuterium gas to the required level, confirmed by the gas chromatography to a precision of $\sim$1 ppb (Sec. 2.3.1).

A complementary method to get the level of chemical impurities is direct impurity detection in the TPC. Following muon capture on nitrogen or oxygen, the recoiling nucleus has a kinetic energy of a few hundred keV, which yields a localized signal in the TPC. The dominant backgrounds in the relevant energy range are $\mu d + d \rightarrow {}^3\mathrm{He} + n$ fusion signals. These are suppressed by a delayed time cut after the muon stop, since the dominant fusion yield comes from the μd quartet state, which depopulates with a lifetime of $\sim$300 ns. In addition, the requirement that no Michel electron is associated with the event further suppresses the ^{3}He background. The remaining fusion background is subtracted by taking the capture-free spectrum (containing events associated with Michel electrons) and normalizing it to the ^{3}He yield. At the increased impurity level of $\sim$20 ppb of nitrogen during the 2013 run, this in-situ method proved to be in excellent agreement with the gas chromatography (Sec. 3.6 in [8]). The improved energy resolution achieved by our new cryogenic preamplifiers [6] proved to be essential.

The same analysis for the 2014 data (Fig. 10) shows that the impurity level during this run is at least 5 times lower than that of the previous year (Fig. 11), which is also confirmed by the gas chromatography (Sec. 2.3.2). The challenge is to determine the possible background contributions in the residual spectrum after the (fusion) background subtraction (Fig. 11).

- **Michel electrons:** The low-energy events in the spectrum (Fig. 10) are dominated by Michel electrons. Due to the geometry of the electron detector, electrons undetected by our electron

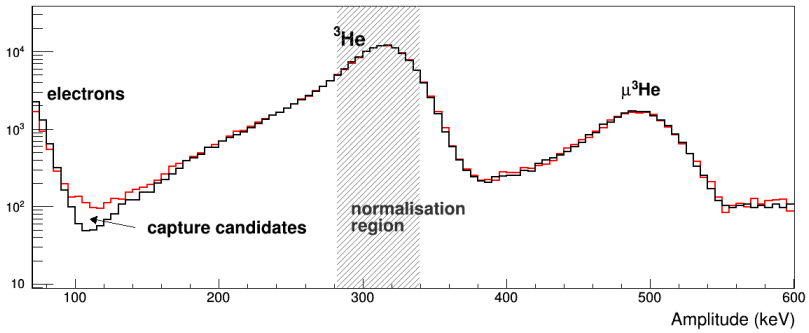

Figure 10: Delayed events at the muon stop position, with a veto on p-t fusions. The fusion background from events associated with a Michel electron (black) is normalized to the ^{3}He yield. There is a excess of counts in the 100-200 keV for events with no associated Michel electron.

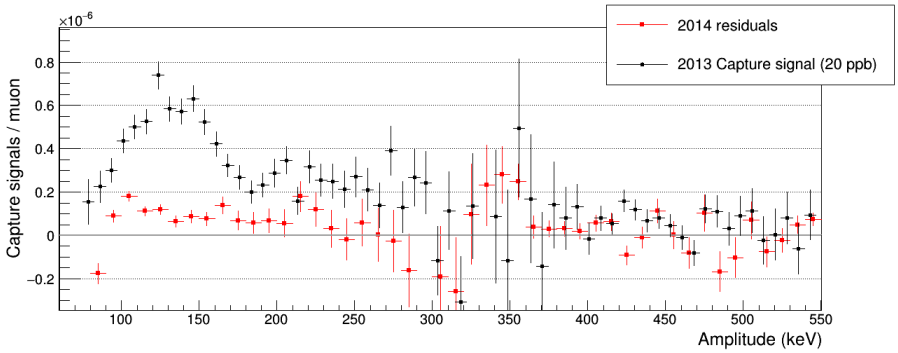

Figure 11: Comparison of the 2013 and 2014 capture recoil candidate spectrum (*red* minus *black* in Fig. 10). Ignoring any background contributions, the residual count in the 100-200 keV region corresponds to 2-3 ppb of nitrogen.

hodoscope have a slightly different signature in the TPC compared to the detected Michel electron. This renders the background subtraction procedure imperfect for Michel electrons. From our μ^+ dataset we could set a limit of 10% or better on the electron contribution to the spectrum in Fig. 11, 100 to 200 keV.

- **Accidental background:** Accidental TPC signals, uncorrelated with the muon, are negligible for this analysis. Small sparks are rejected by their characteristic signature in the TPC.
- **Capture neutron background:** Neutrons from μd capture can scatter in the TPC. Such a signal has the same signature as a nuclear recoil from muon capture on gas impurities: a localized energy deposition with no associated Michel electron. A first Monte-Carlo estimate showed that the signal yield of these capture neutrons in the TPC is comparable to the capture yield for ppb-level impurities (Tab. 4).

At the end of the 2014 run, the temperature of the TPC was decreased from 31 K to 28 K. The nitrogen concentrations at the vapor pressure for these temperature are 20 ppb and 1 ppb, respectively. The observed capture yield did not change significantly. This confirms the hypothesis that μd captures make up most of the signal. This capture neutron background will be determined by measuring the yield away from the muon stop position, and scaling it back with the help of our Monte Carlo code. After subtracting this background, the residual impurity signal will be combined with the 20 ppb data and the

2 ppm N_2 doped data from 2013 to zero-extrapolate the measured lifetime.

	calculated yield per muon	expected yield after analysis cuts
^{3}He	$2.8\ 10^{-2}$	$16\ 10^{-6}$
μ-N capture per ppb	$2.4\ 10^{-6}$	$0.6\ 10^{-6}$
neutrons from μd capture	10^{-3}	$0.4\ 10^{-6}$

Table 4: Expected yields of ^{3}He fusions, muon captures on nitrogen and neutrons from μd capture per muon, using the relative density Φ=0.06 of R2014 and the kinetic parameters listed in [10]. The *analysis cuts* are energy depositions between 100 and 200 keV in a 3-8 μs delayed window. The quoted neutron yields are preliminary, estimated with our GEANT4 code.

3.3.2 Interferences

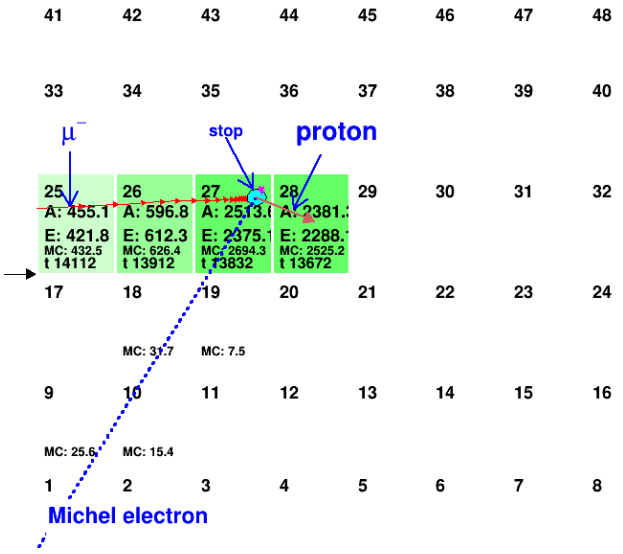

Figure 12: TPC pad display. The basic tracking algorithm would identify pad 28 as the muon stop pad, but the fusion-threshold based tracker will pick pad 27, because the pulse energy is above threshold due to the proton and triton.

To minimize effects of d + d fusion on the measured μ^- decay rate we make the muon stop definition as insensitive to the fusion products as possible. The most basic muon tracking algorithm derives the muon stop coordinates from the most downstream pulse in a cluster of pulses in the TPC. The Z and X coordinates are determined by the pad on which the charge pulse arrives, and the Y coordinate is calculated from the drift time. The deficiencies of this algorithm are that delayed fusion products can shift the reconstructed drift time of the pulse, or deposit charge in a nearby pad, confusing the Z or X determination. We have tested a different algorithm that uses a threshold *fusion energy*, set to be larger than the maximum energy a muon alone can deposit in one pad. The Z coordinate is given by the pad whose pulse energy exceeds this threshold (*fusion pad*). For upstream-going protons, this fusion pad may not be the most downstream pad in the track. The Y coordinate is extrapolated using only pulses in pads upstream of the fusion pad. To determine the Y coordinate of the pulse, we extrapolate along the *road* of pulses on pads upstream of the fusion pad. This greatly reduces the possibility for a fusion product to confuse the Y coordinate, at the expense of reduced Y resolution.

We study fusion interference in detail using Monte Carlo data samples where we keep track of all the essential Monte Carlo truth information. For these studies we run GEANT as normal, but in the

detector response we discard muon stops that did not have at least one fusion in the active TPC volume. This gives us a highly enriched sample of muon stops with the correct number of single, double or triple fusions per stop. We reconstruct these events, tuning the muon stop definition algorithm by comparing the reconstructed stop point with the Monte Carlo truth.

As a first step we look at event displays with Monte Carlo truth overlaid on the reconstructed information. We are most concerned with events that have a $\mathrm{p}+\mathrm{t}$ fusion as the proton will travel 16 mm and therefore will often leave the stop pad. An example of such an event is shown in Fig. 12. The reconstructed amplitude and energy are shown in each pad along with the Monte Carlo energy deposited. The incoming muon steps are shown in red with the stop position drawn as a blue circle and proton tracks as brown arrows. The out-going Michel electron (dashed blue line) typically does not deposit enough energy to trigger the readout, although this depends on the threshold as well as the electronic noise. We observe that for these events the 1 MeV triton deposits its energy in the stop pad. In some cases it is not clear whether the fusion products caused a misreconstruction, and it is useful to run the same events through the detector response excluding the fusion products but keeping the same random noise.

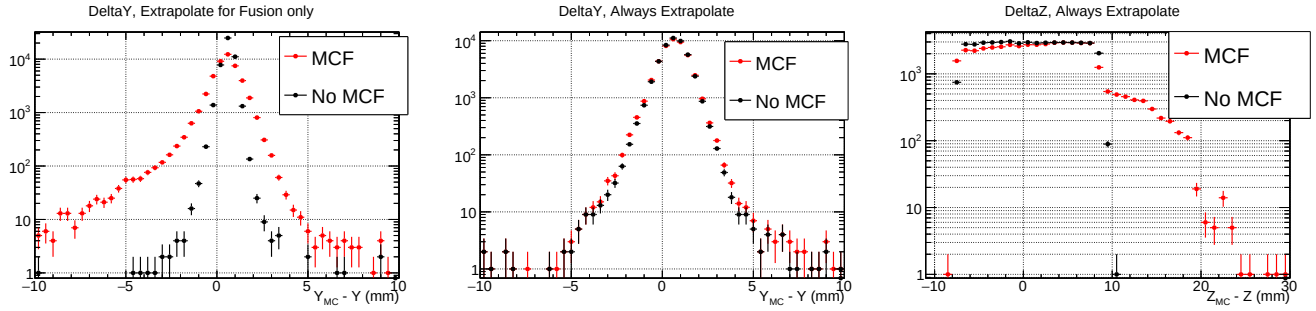

Figure 13: Comparison of algorithms for determining the coordinates of the muon stop using MC data. The difference between reconstruction and truth is shown for algorithms that extrapolate into the most downstream pad to determine Y. The black points are from control data where the energy deposition of muon-catalyzed fusion (MCF) products is removed in the simulation. In the left figure, the extrapolation is done for only tracks with enough energy in the last pad to reliably indicate a MCF event. In the center figure, extrapolation is performed for all tracks, removing any discrepancy. Examining the Z-coordinate (right), however, shows that a large discrepancy still exists.

After a basic tune using event displays, we histogram differences in reconstructed versus true stop positions. We are interested in cases where the fusion moves the reconstructed stop point, as that will cause some events to cross fiducial volume boundaries. We use events where we have removed the fusion products from the detector simulation as well as simulated μ^+ data samples to determine our stop resolution. We observe that for the X stop position the fusion products have little if any effect. However, improvement is observed in the reconstruction of the Y coordinate. In Fig. 13, the left panel shows the distribution of reconstructed Y values relative to the MC true stop coordinate. The resolution is worse when the Y value is determined via extrapolation, but there is also a tail corresponding to $\mathrm{d}\mu^-\mathrm{d} \rightarrow \mu^- + \mathrm{n} + {}^3\mathrm{He}$ events where the ^{3}He energy deposition was too low to trigger the threshold. A variation on the projection algorithm, where extrapolation is used to determine Y for all tracks, removes nearly all of the discrepancy between data with fusion products and without (Fig. 13, left).

The biggest remaining concern is $\mathrm{p}+\mathrm{t}$ fusions where the proton travels to a pad other than the muon stop pad. In Fig. 13, one can see that the reconstructed Z coordinate is minimally affected by the choice of Y projection algorithm and a large tail remains where the proton goes upstream, causing the upstream pad to go above the fusion energy. To ameliorate this, we are attempting to discriminate forward-going from backward-going protons using the distribution of energy on the final two pads and manipulate the stopping distribution to balance the events that leave and enter the fiducial volume due to the proton energy deposition.

4 Beam Time Request 2015

In 2015 we request beam time for the second major MuSun production run in πE1. The optimal time window would be a 12-week block from July 6 to September 28. We need to run during the summer months; otherwise key faculty cannot participate. Without their expertise we cannot efficiently start a major, and potentially final, MuSun production run. Last year we urged the PAC, the PSI management and our μSR colleagues for such a schedule, which was generously granted. The result was a highly successful experimental run. We also request unrestricted access to the πE1.2 area 3 weeks in advance of the run.

- 2 weeks: Commissioning and optimization of all parameters (beam, chambers) for highly efficient production.
- 9 weeks: Production to collect a statistics of about 8×10^9 $\mu^- - e$ events and 1×10^9 $\mu^+ - e^+$ events. Here events refer to fully reconstructed pairs that pass all final analysis cuts.
- 1 week: Systematic measurements, including purity studies. We plan to use the the newly-developed dynamic impurity calibration method inside the TPC to simultaneously cross-calibrate the gas chromatography and the recoil method.

References

[1] MuSun Collaboration (http://muon.npl.washington.edu/exp/MuSun): V.A. Andreev, E.J. Barnes, R.M. Carey, V.A. Ganzha, A. Gardestig, T. Gorringe, F.E. Gray, D.W. Hertzog, M. Hildebrandt, L. Ibanez, P. Kammel, B. Kiburg, S.A. Kizilgul, S. Knaack, P.A. Kravtsov, A.G. Krivshich, K. Kubodera, B. Lauss, M. Levchenko, X. Luo, K.R. Lynch, E.M. Maev, O.E. Maev, F. Mulhauser, M.H. Murray, F. Myhrer, K. Neely, A. Nadtochy, C. Petitjean, G.E. Petrov, J. Phillips, R. Prieels, D. Prindle, N. Raha, R. Ryan, G.N. Schapkin, N. Schroeder, G.G. Semenchuk, M.A. Soroka, V. Tishchenko, A.A. Vasilyev, A.A. Vorobyov, N. Voropaev, M.E. Vznuzdaev, F. Wauters, P. Winter.

[2] Andreev, V. et al. *Phys. Rev. Lett.* **110**, 012504 (2013).

[3] Egger, J., Fahrni, D., Hildebrandt, M., Hofer, A., Meier, L., Petitjean, C., Andreev, V., Banks, T., Clayton, S., Ganzha, V., Gray, F., Kammel, P., Kiburg, B., Kravtsov, P., Krivshich, A., Lauss, B., Maev, E., Maev, O., Petrov, G., Semenchuk, G., Vasilyev, A., Vorobyov, A., Vznuzdaev, M., and Winter, P. *The European Physical Journal A* **50**(10) (2014).

[4] Tishchenko, V. et al. *Phys. Rev.* **D87**(5), 052003 (2013).

[5] Kammel, P. and Kubodera, K. *Annu. Rev. Nucl. Part. Sci.* **60**, 32753 (2010).

[6] Ryan, R. A., Wauters, F., Gray, F. E., Kammel, P., Nadtochy, A., Peterson, D., van Wechel, T., Gross, E., Gubanich, M., Kochenda, L., Kravtsov, P., Orozco, D., Osofsky, R., Murray, M. H., Petrov, G. E., Phillips, J. D., Stroud, J., Trofimov, V., Vasilyev, A., and Vznuzdaev, M. *Journal of Instrumentation* **9**(07), P07029 (2014).

[7] Ganzha, V. A. et al. *Nucl. Instrum. Meth.* **A578**, 485–497 (2007).

[8] MuSun Collaboration. (2014). Progress Report 2013 and Beam Request for 2014.

[9] Kravtsov, P. and Trofimov, V. *Preprint PNPI-2723* (2014). lkst.pnpi.nw.ru/uploads/pubs/preprints/daq32_preprint.pdf.

[10] Andreev, V. et al. (2010). arXiv:1004.1754.